Dynamic Stability of Repeated Agent-Environment Interactions During the Hybrid Ball-bouncing Task

Guillaume Avrin[1,2,3], Maria Makarov[1], Pedro Rodriguez-Ayerbe[1] and Isabelle A. Siegler[2,3]

[1]*Laboratoire des Signaux et Systèmes (L2S), CentraleSupélec - CNRS - Univ. Paris-Sud, Université Paris-Saclay, Plateau du Moulon, 3 Rue Joliot Curie, F-91192 Gif-sur-Yvette, France*

[2]*CIAMS, Univ. Paris-Sud, Université Paris-Saclay, 15 Rue Georges Clemenceau, 91405 Orsay, France*

[3]*CIAMS, Université d'Orléans, Château de la Source, Avenue du Parc Floral, 45067 Orléans, France*

Keywords: Hybrid System, Bouncing Ball, Stability, Impact Map, Biologically-inspired Control.

Abstract: This interdisciplinary study aims to understand and model human motor control principles using automatic control methods, with possible applications in robotics for tasks involving a rhythmic interaction with the environment. The paper analyses the properties of a candidate model for the visual servoing of the 1D bouncing ball benchmark task in humans. The contributions are twofold as they *i/* enable a computationally efficient way of testing hypotheses in human motor control modeling, and *ii/* will allow to export and adapt the lessons learned from this modeling of human behavior for more robust and less model-dependent robotic control methods. Three hypotheses about the sensorimotor couplings involved during the task, i.e. three control structures are analyzed from the point of view of task stability by means of Poincaré maps. Obtained results are used to refine the proposed models of sensorimotor couplings. It is shown that the fixed points of the Poincaré maps are stable and that the obtained linear approximation, derived on these equilibrium points, can be viewed as a state-feedback. As such, the human-like controller is compared to the Linear Quadratic controller around the equilibrium point.

1 INTRODUCTION

Visual servoing of one-dimensional ball bouncing is a well-known benchmark in neuroscience and robotics (Kulchenko and Todorov, 2011), (Sternad et al., 2001), (Williamson, 1999). This apparently simple but hybrid task presents coordination constraints which are well mastered by humans but still excessively hard to manage for robots. A room for improvement in the creation of robots capable of human-like performances thus remains. The present study intends to show that the use of automatic control methods and particularly those related to stability analysis can lead to a deaper understanding of the key principles allowing humans to efficiently adapt behavior to the environment. Past studies in neuroscience have shown that a neural network, known as Central Pattern Generator (CPG), is present at the spinal level in vertebrates to generate basic rhythmic movements for tasks such as locomotion and respiration. The output of the most common CPG models can be considered as sinusoidal in first approximation (Yu et al., 2014).

To design a model with a structure close to the one of the human central nervous system, some roboticists, including the authors, have proposed control architectures based on neural oscillators producing quasi-sinusoidal trajectories to stabilize the bouncing task (Avrin et al., 2016), (de Rugy et al., 2003), (Williamson, 1999). The stability analysis of such hybrid systems generally relies on Poincaré impact maps. These analyses have been well documented for open-loop stabilization of ball bouncing (Buehler et al., 1990), (Dijkstra et al., 2004), (Holmes, 1982), (Vincent, 1995) and frequency control of the task (Choudhary, 2016), (Vincent and Mees, 2000), but no stability analysis of controllers modulating simultaneously the frequency and amplitude of the movement was found by the authors.

The present paper analyzes the recently identified period and amplitude adaptation laws used by humans to achieve the ball-bouncing task (Siegler et al., 2013). The ball bouncing dynamics under these human control strategies are shown to be accurately modeled by a nonlinear singular Poincaré impact map involving an implicit partial differential algebraic equation solved numerically. Linear analysis

around equilibrium points is used to study the stability of the control strategies. We show that a stable behavior is obtained and that the human-like controller can be seen as an Optimal Linear Quadratic Regulator (LQR) around the equilibrium point. The study leads to the conclusion that the method can be used to efficiently tune CPG-based controllers for robotic applications while reducing the computational time allocated to the simulation of the continuous dynamics of the system. The ball bouncing task and its equations are presented in Section 2. Section 3 analyzes the stability of the bio-inspired controller with amplitude and frequency control. In Section 4, the implicit map is approximated by an explicit one and the influence of this approximation on the stability properties is analyzed. In Section 5, the approximated bouncing map is compared to a LQR controller within the spirit of the one proposed for frequency control in (Vincent and Mees, 2000) but for the paddle oscillation amplitude control. The Poincaré map with active phase control is analyzed in Section 6. The results are discussed and conclusions drawn in Section 7.

2 BALL BOUNCING TASK

2.1 Poincaré Maps of the Ball-Bouncing Task

The considered 1D ball-bouncing task is represented on Figure 1. The agent handles a paddle and moves his/her arm to bounce a ball in the vertical direction. During each cycle, the paddle oscillation period T_r and amplitude A can be adapted to control the ball trajectory. The ball flight between two impacts at t_k and t_{k+1} is governed by ballistic equations:

$$\left. \begin{array}{l} x(t) = x_k + V_k(t - t_k) - 0.5g(t - t_k)^2 \\ V(t) = V_k - g(t - t_k) \end{array} \right\} \text{ for } t_k < t < t_{k+1}$$

$$(1)$$

with $x(t)$ and $V(t)$ the ball position and velocity, t_k the impact instant, x_k the impact position, V_k the ball velocity directly after impact, and g the gravity acceleration. Considering that the ball mass is negligible in comparison with the paddle mass, and that the impacts are instantaneous, the impact equation is (Dijkstra et al., 2004), (Ronsse and Sepulchre, 2006):

$$V_{k+1} = -\alpha V_{k+1}^- + (1+\alpha)V_{r_{k+1}} \tag{2}$$

with α the ball-paddle restitution coefficient at impact ($\alpha \in \,]0,1[$), $V_{r_{k+1}}$ the paddle velocity at impact, V_{k+1}^-

the ball velocity directly before impact $k+1$. According to the ballistic trajectory of the ball, $V_{k+1}^- = V_k - g(t_{k+1} - t_k)$.

It is considered that the paddle oscillates vertically. The displacement from the origin is noted $r(t)$. Between impacts k and $k+1$, if the trajectory of the paddle is sinusoidal, $r(t)$ is given by: $r(t) = A_{k+1}\sin(\omega_{k+1}(t - t_k) + \phi_k)$. When the paddle oscillation frequency is modified by the controller at impact $k+1$, the oscillation phase remains continuous:

$$\phi_{k+1} = \omega_{k+1}(t_{k+1} - t_k) + \phi_k \tag{3}$$

The paddle velocity at impact $k+1$ is thus equal to $A_{k+1}\omega_{k+1}\cos(\omega_{k+1}(t_{k+1} - t_k) + \phi_k)$, which is equal to $A_{k+1}\omega_{k+1}\cos(\phi_{k+1})$. As a consequence, according to (1) and (2), for $t = t_{k+1}$, the ball bouncing can be described by an autonomous discrete-time nonlinear system presented in (4), Equation (4b) being an implicit equation.

$$V_{k+1} = -\alpha V_k + (1+\alpha)A_{k+1}\omega_{k+1}\cos(\phi_{k+1})$$
$$+ \alpha g(t_{k+1} - t_k) \tag{4a}$$
$$A_{k+1}\sin(\phi_{k+1}) = A_k\sin(\phi_k) + V_k(t_{k+1} - t_k)$$
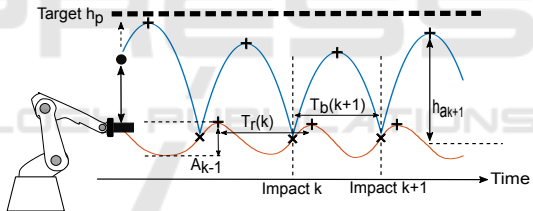$$- g/2(t_{k+1} - t_k)^2 \tag{4b}$$

Figure 1: The ball-bouncing task.

2.2 Human Control of Ball Bouncing

In the ball-bouncing task of the present paper, a predefined target height h_p is considered (see Figure 1). Siegler et al. revealed that at each cycle, humans adapt the paddle period to be equal to the ball period (5a). To cancel the bounce error $\varepsilon_k = h_p - h_{a_k}$, with h_{a_k} the ball apex at cycle k, they adapt the paddle velocity from previous impact proportionally to ε_k (Siegler et al., 2013). The assumption is made in the present paper that this error correction is achieved via an adaptation of the paddle oscillation amplitude:

$$T_r(k+1) = T_b(k+1) = 2V_k/g \tag{5a}$$
$$\Delta A(k+1) \hat{=} A_{k+1} - A_k = \lambda\varepsilon_k \tag{5b}$$

with λ a positive scalar and $T_b(k+1)$ the ball period during the cycle directly after impact k.

In addition to these adaptation strategies, experimental studies showed that the human behavior is settled around a passive stability regime characterized by a specific interval of negative paddle accelerations at impact, as evidenced by the stability analysis of the open-loop task dynamics (Schaal et al., 1996), (Tufillaro et al., 1986). Previous studies have hypothesized that sensory information is used by humans to allow the bounce to stay or to return to this passive stability regime (Morice et al., 2007), (de Rugy et al., 2003), (Siegler et al., 2010). The present study hypothesizes that this convergence towards the passive stability regime is the result of an active control of the impact phase. The influence of these amplitude, frequency and phase adaptation strategies on the task stability is analyzed throughout the paper.

2.3 Bio-inspired Controllers

In the next sections, the study of the different bio-inspired controllers is achieved by analyzing the following discrete-time representations:

- Map with amplitude and frequency control (Section 3.1)
- Approximated map with amplitude and frequency control (Section 4)
- Map with amplitude, period and phase control (Section 5)

These representations model the discrete dynamics of the task controlled by the human CPG, that is viewed as a generator of sinusoidal trajectories. The additional dynamics introduced by the agent's arm mechanical system are supposed to be accurately canceled by low-level tracking controllers, such as a PID controller in Figure 2. The arm dynamics are thus not considered in the present paper. All the presented results have been achieved for $g = 9.81 m/s^2$ and $h_p = 0.55m$.
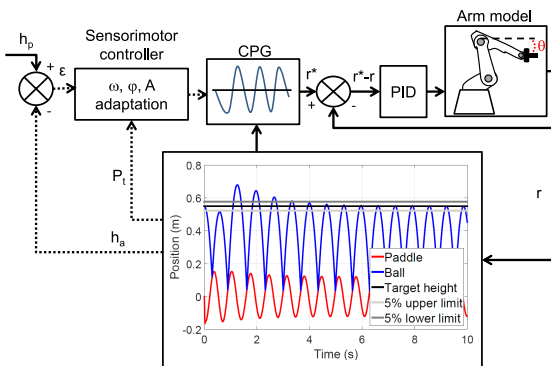

Figure 2: Block diagram of the ball bouncing closed-loop.

3 HUMAN-LIKE BOUNCING MAP

In this section, the Poincaré map with amplitude and frequency control is derived and its stability analyzed.

3.1 Map Definition and Equilibrium Points

In this case, the Poincaré map of (4) holds, but the amplitude A_k varies according to (5b). The ball apex is given by $h_{a_k} = V_k^2/(2g) + A_k \sin(\phi_k)$. The paddle frequency being controlled by $\omega_{k+1} = \pi g/V_k$, the bouncing map is:

$$A_{k+1} = A_k + \lambda(h_p - A_k \sin(\phi_k) - \frac{V_k^2}{2g}) \quad (6a)$$

$$V_{k+1} = -\alpha V_k + (1+\alpha)A_{k+1}\frac{\pi g}{V_k}\cos(\phi_{k+1})$$
$$+ \alpha\frac{V_k}{\pi}(\phi_{k+1} - \phi_k) \quad (6b)$$

$$A_{k+1}\sin(\phi_{k+1}) - A_k\sin(\phi_k) - \frac{V_k^2}{\pi g}(\phi_{k+1} - \phi_k)$$
$$+ \frac{V_k^2}{2\pi^2 g}(\phi_{k+1} - \phi_k)^2 = 0 \quad (6c)$$

For $\bar{\phi}$ solution of (6c), such that $\phi_{k+1} = \bar{\phi} + 2\pi$, the equilibrium point of (6) is given by considering $V_{k+1} = V_k = \bar{V}$ and $A_{k+1} = A_k = \bar{A}$:

$$\bar{A} = \frac{h_p}{\frac{(1+\alpha)\pi\cos(\bar{\phi})}{2(1-\alpha)} + \sin(\bar{\phi})}, \quad \bar{V} = \sqrt{\frac{(1+\alpha)\bar{A}\pi g\cos(\bar{\phi})}{(1-\alpha)}} \quad (7)$$

It can be noted that no equilibrium point exists for $\bar{\phi}$ in $]\pi/2, 3\pi/2[$ as $\bar{V}$ would be undefined. In addition, only the realistic (positive) values of the paddle amplitude are considered. For $\bar{A}$ to be positive, $\bar{\phi}$ must be inside the interval $]\phi_{lim}, \pi/2[$ with the limit phase value ϕ_{lim} given by:

$$\phi_{lim} = \arctan\left(\frac{-(1+\alpha)\pi}{2(1-\alpha)}\right) \quad (8)$$

Figure 3 presents a comparison between the trajectory variables A_k and V_k as functions of the impact number k, predicted by the bouncing map (6) or resulting from the numerical simulations of the continuous ball and paddle trajectories. The figure illustrates the good matching between the predicted and simulated variables and underlines the interest of analyzing the task stability properties by focusing on the presented Poincaré section corresponding to the ball-paddle impact.

3.2 Linear Stability Analysis

The Jacobian matrix of (6) is given by:

$$J = \begin{pmatrix} \frac{\partial A_{k+1}}{\partial A_k} & \frac{\partial A_{k+1}}{\partial V_k} & \frac{\partial A_{k+1}}{\partial \phi_k} \\ \frac{\partial V_{k+1}}{\partial A_k} & \frac{\partial V_{k+1}}{\partial V_k} & \frac{\partial V_{k+1}}{\partial \phi_k} \\ \frac{\partial \phi_{k+1}}{\partial A_k} & \frac{\partial \phi_{k+1}}{\partial V_k} & \frac{\partial \phi_{k+1}}{\partial \phi_k} \end{pmatrix} \quad (9)$$

with the partial derivatives given by:

$$\frac{\partial A_{k+1}}{\partial A_k} = 1 - \lambda \sin(\phi_k), \quad \frac{\partial A_{k+1}}{\partial V_k} = -\frac{\lambda V_k}{g}$$

$$\frac{\partial A_{k+1}}{\partial \phi_k} = -\lambda A_k \cos(\phi_k)$$

$$\frac{\partial V_{k+1}}{\partial A_k} = (1+\alpha)\frac{\pi g}{V_k}(\cos(\phi_{k+1})\frac{\partial A_{k+1}}{\partial A_k}$$
$$- A_{k+1}\sin(\phi_{k+1}\frac{\partial \phi_{k+1}}{\partial A_k})) + \frac{\alpha V_k}{\phi_k}\frac{\partial \phi_{k+1}}{\partial A_k}$$

$$\frac{\partial V_{k+1}}{\partial V_k} = (1+\alpha)\pi g(\frac{\frac{\partial A_{k+1}}{\partial V_k}V_k - A_{k+1}}{V_k^2}\cos(\phi_{k+1})$$
$$- \frac{A_{k+1}}{V_k}\frac{\partial \phi_{k+1}}{\partial V_k}\sin(\phi_{k+1})) - \alpha \quad (10)$$
$$+ \frac{\alpha}{\pi}(\phi_{k+1} - \phi_k + V_k\frac{\partial \phi_{k+1}}{\partial V_k})$$

$$\frac{\partial V_{k+1}}{\partial \phi_k} = (1+\alpha)\frac{\pi g}{V_k}(\frac{\partial A_{k+1}}{\partial \phi_k}\cos(\phi_{k+1})$$
$$- A_{k+1}\frac{\partial \phi_{k+1}}{\partial \phi_k}\sin(\phi_{k+1}))$$
$$+ \frac{\alpha V_k}{\pi}(\frac{\partial \phi_{k+1}}{\partial \phi_k} - 1)$$

$$\frac{\partial \phi_{k+1}}{\partial A_k} = -\frac{\partial F/\partial A_k}{\partial F/\partial \phi_{k+1}}, \quad \frac{\partial \phi_{k+1}}{\partial V_k} = -\frac{\partial F/\partial V_k}{\partial F/\partial \phi_{k+1}}$$

$$\frac{\partial \phi_{k+1}}{\partial \phi_k} = -\frac{\partial F/\partial \phi_k}{\partial F/\partial \phi_{k+1}}$$

with F being the left-hand side of the implicit Equation (6c).

The Jacobian matrix J in (9) is evaluated at the equilibrium point (7) and its eigenvalues are denoted ev_1, ev_2, ev_3. It can be shown that ev_1 and ev_2 are two hyperbolic eigenvalues. ev_2 is stable ($|ev_2| < 1$), for any value of α and λ whereas ev_1 has a stability that essentially depends on the value of λ. These results are demonstrated in the next Section when compared to the ones of the approximated map. On the contrary, ev_3 was shown to be independent of the values of α and λ, and always equal to unity. ev_3 is thus non-hyperbolic but also non-defective. It is thus possible to conclude that the linearized system is Lyapunov stable, but nothing can be directly deduced for the nonlinear Poincaré map stability (Stuart and Humphries, 1998). The bouncing map (6) is thus singular. Indeed, in addition to the fact that $ev_3 = 1$, it
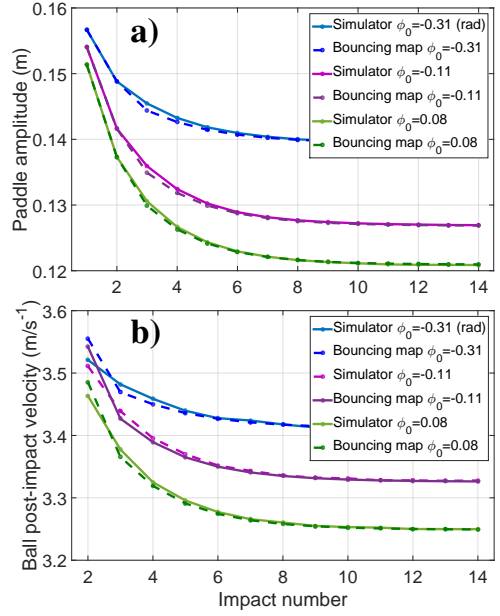

Figure 3: Comparison of the bouncing map predictions and simulation of a) the amplitudes series and b) the ball post-impact velocity series. Three values of the the initial impact phase ϕ_0 ($\lambda = 0.09$) are considered.

can be seen that (6) is identically zero for any steady-state value of $\bar{\phi}$. Numerical simulations suggest that the continuum of equilibrium points defined by relations (7), with $\bar{\phi}$ a free variable in $]\phi_{lim}, \pi/2[$, is stable. During simulated trials, the value of $\bar{\phi}$ was also shown to vary only slightly from its initial value ϕ_0, which lead us to the approximation presented in the next Section.

4 THE HIGH BOUNCE MAP APPROXIMATION

The implicit equation of the bouncing map presented in the previous section is approximated by an explicit equation in the present section to simplify the stability analysis. The validity of the approximation is confirmed by comparison with numerical simulations.

4.1 Approximated Bouncing Map and Equilibrium Points

In order to provide an explicit form to the time map (4b), the *high bounce approximation* is commonly considered. This approximation supposes that the paddle displacement amplitude is small compared to the ball apex (Holmes, 1982), (Vincent and Mees, 2000), (Vincent, 1995). In that case, one has $V_{k+1}^- =$

$-V_k$. As $V_{k+1}^- = V_k - g(t_{k+1} - t_k)$, the time map of the high bounce approximation is given by $t_{k+1} - t_k \approx 2V_k/g$. As a consequence, according to (2), the ball velocity after impact is given by: $V_{k+1} = \alpha V_k + (1 + \alpha)V_{r_{k+1}}$. The high bounce map (HBM) with frequency and amplitude control is:

$$V_{k+1} = \alpha V_k + (1+\alpha)A_{k+1}\omega_{k+1}\cos(\phi_{k+1}) \tag{11a}$$

$$A_{k+1} = A_k + \lambda(h_p - A_k\sin(\phi_k) - V_k^2/(2g)) \tag{11b}$$

and $\bar{\phi}$ is given by the trivial phase map $\phi_{k+1} = \phi_k + 2\pi$ and thus $\bar{\phi} = \phi_0 (mod\,2\pi)$.

This approximated bouncing map is compared to numerical simulations of the complete system continuous dynamics for validation. Let V_0, A_0 and ϕ_0 be the initial state values of (11). For different values of λ and specific initial and environmental conditions, Figure 4a) compares the transient evolution of the ball apex h_a of the simulated solution of (6) to the one calculated with the high bounce map (11). It can be seen that the dynamics of the task are well described by the proposed approximated map, and that changing the value of λ does not modify the equilibrium but changes the task transient dynamics. Figure 4b) shows that when V_0 changes, the equilibrium point is not modified and it can be seen that the simulations indeed converge towards $\bar{V}$ calculated thanks to relation (7). Figure 4c) shows that, as expected, when ϕ_0 is modified, the equilibrium point is modified and is well predicted by (7).

By simulation, it was observed than ϕ varied by less than 10% of its initial value ϕ_0 during trials, for values of ϕ_0 inside $[-\pi/4, 2\pi/5]$. As a consequence, the high bounce approximation is acceptable for this interval. The reader should nevertheless keep in mind that outside this interval, the high bounce map modeling accuracy decreases even if the whole phase interval $]\phi_{lim}, \pi/2[$ is considered for the stability analysis presented bellow. This accuracy limitation does not prevent the method to provide information about the human behavior as it was observed experimentally that almost all the impact phases of humans were in $[-\pi/4, 2\pi/5]$ (Sternad et al., 2001), (Siegler et al., 2010).

4.2 Linear Stability Analysis

The Jacobian matrix of (11) is given by:

$$J = \begin{pmatrix} \frac{\partial A_{k+1}}{\partial A_k} & \frac{\partial A_{k+1}}{\partial V_k} \\ \frac{\partial V_{k+1}}{\partial A_k} & \frac{\partial V_{k+1}}{\partial V_k} \end{pmatrix} \tag{12}$$

with the partial derivatives given by:

$$\frac{\partial A_{k+1}}{\partial A_k} = 1 - \lambda\sin(\phi_k) \tag{13a}$$

$$\frac{\partial A_{k+1}}{\partial V_k} = -\frac{\lambda V_k}{g} \tag{13b}$$

$$\frac{\partial V_{k+1}}{\partial A_k} = \frac{-\pi g\cos(\phi_{k+1})(\alpha+1)(\lambda\sin(\phi_k)-1)}{V_k} \tag{13c}$$

$$\frac{\partial V_{k+1}}{\partial V_k} = \alpha - \pi\lambda\cos(\phi_{k+1})(\alpha+1)$$
$$- \frac{\pi g\cos(\phi_{k+1})(\alpha+1)(A_k + \lambda(h_p - h_{a_k}))}{V_k^2} \tag{13d}$$

J evaluated at the equilibrium point is thus equal to (with $\bar{\phi} = \phi_0 (mod\,2\pi)$):

$$J^* = \begin{pmatrix} 1 - \lambda\sin(\bar{\phi}) & -\frac{\lambda\bar{V}}{g} \\ \frac{-\pi g\cos(\bar{\phi})(\alpha+1)(\lambda\sin(\bar{\phi})-1)}{\bar{V}} & 2\alpha - \pi\lambda\cos(\bar{\phi})(\alpha+1) - 1 \end{pmatrix} \tag{14}$$

The eigenvalues of J^* have a complex expression that will not be presented in the present paper. The influence of α, λ and ϕ_0 on the system linear stability is analyzed in the following paragraphs.

4.3 Influence of the High Bounce Approximation on the Stability

Figure 5 represents the influence of λ and $\bar{\phi}$ on the two hyperbolic eigenvalues $|ev_1|$ and $|ev_2|$, for $\alpha = 0.48$ and $\bar{\phi}$ in $]\phi_{lim}, \pi/2[$. As mentioned in Section 3.2, it can be seen that ev_2 is always stable whereas the stability of ev_1 depends on the value of λ, that has to be lower than 0.4 for the system to be asymptotically stable for any value of $\bar{\phi}$. For appropriate value of λ, ev_1 and ev_2 are thus hyperbolic stable. For $\bar{\phi}$ inside the considered interval $]\phi_{lim}, \pi/2[$ and away from the extreme values, the stability prediction of the approximated map, with the limit λ value equal to 0.4, matches the one of the high bounce map. This validity interval is acceptable considering that the human bouncing phase is localized in the interval $[-\pi/4, 2\pi/5]$ as recalled in Section 4.1.

Finally, even if stable, the bouncing maps (6) and (11) have transient dynamics that depends greatly on the value of α, as shown in Figure 6. Indeed, the equilibrium node shape is a stable hyperbolic node for α around 0.1 (Figure 6a) and b), real eigenvalues and $-1 < ev_1 < ev_2 < 1$), a stable one-tangent node for α around 0.55 ($-1 < ev_1 = ev_2 < 1$) and a stable spiral (elliptic point) for α around 0.9 (Figure 6c) and d), ev_1 and ev_2 complex, conjugate and $|ev_1| = |ev_2| < 1$). The influence of α on the eigenvalues real parts and imaginary parts of the approximated and non-approximated maps is evidenced in Figure 7. It can be noted that this influence is very similar
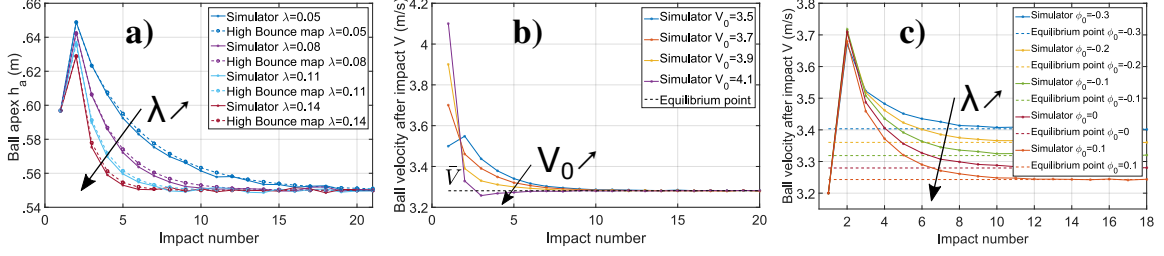
Figure 4: Evolution of a) the ball apex for different values of λ ($V_0 = 3.2$, $\phi_0 = \pi/6$) b) the ball velocity after impact for different values of V_0 ($\lambda = 0.09$, $\phi_0 = \pi/6$) and c) the ball velocity after impact for different values of ϕ_0 ($V_0 = 3.2$, $\lambda = 0.09$). The three graphs are represented as a function of the impact number. For each simulation, $\alpha = 0.48$, $A_0 = 0.15$.
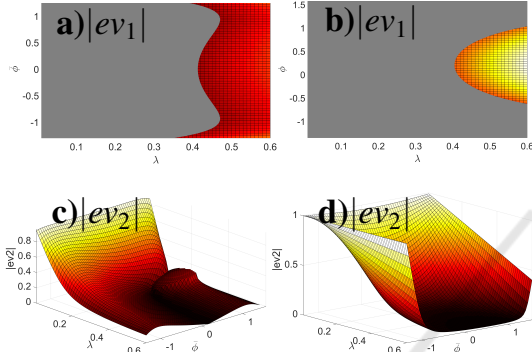

Figure 5: Left column concerns the non-approximated map and right column the high bounce map. a) and b) represent $|ev_1|$. c) and d) represent $|ev_2|$. Eigenvalues are plotted as a function of $\bar{\phi}$ and λ. The grey area on Figures a) and b) corresponds to $|ev| < 1$ (stable area). The Figures c) and d) are represented in 3D plots as the second eigenvalue is always lower than unity.

for the high bounce map and non-approximated map, confirming the pertinence of the approximation.

As a particular case of the previously presented Poincaré maps with amplitude and frequency control, one can notice that if only the period is controlled while the amplitude remains constant, then the approximated and non-approximated maps are identical. They have one trivial eigenvalue equal to 1, corresponding to the relation $\phi_{k+1} = \phi_k + 2\pi$, and one eigenvalue equal to $2\alpha - 1$ that is hyperbolic stable as $\alpha \in {]}0, 1{[}$. The system is thus linearly (asymptotically) stable regardless of the environmental conditions.

4.4 Estimation of the Attraction Domain

For the approximated and non-approximated maps, if the value of the paddle amplitude A is not forced to be positive, the domain of initial conditions leading to a stable bouncing and a convergence towards the equilibrium point of (7) depends on the values of α, g, λ
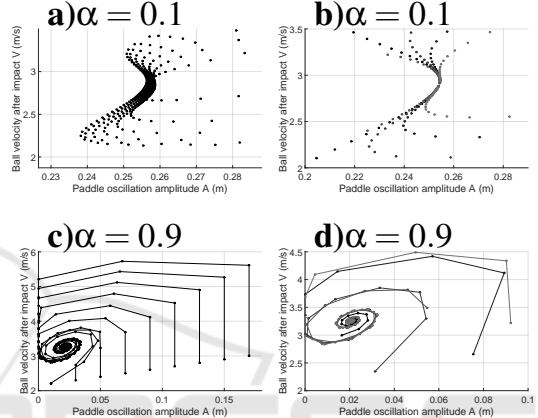

Figure 6: Left column concerns the non-approximated map and right column the high bounce map. Nodes shapes a) and b) for $\alpha = 0.1$, c) and d) for $\alpha = 0.9$ and A forced to be non-negative ($\lambda = 0.09$, $\phi_0 = 0.5$, $A_0 = 0.15$).
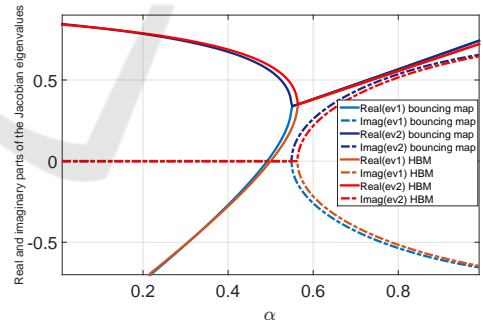

Figure 7: Real and imaginary parts of the approximated (red lines) and non-approximated (blue lines) Jacobian eigenvalues, as functions of α ($\lambda = 0.09$, $\bar{\phi} = 0.5$).

and $\bar{\phi}$. For a specific equilibrium point defined by $\bar{\phi}$, the attraction domain can be estimated by uniformly selecting pairs of initial conditions values $\{V_0, A_0\}$ and analyzing the corresponding steady-state behavior (stable or chaotic). This estimation of the stability domain was achieved for both the approximated and non-approximated maps, and they were shown to be the same. As a consequence, Figure 8 only shows the resulting attraction domain for the non-approximated

map. The region of the figure with the superimposed stable and unstable areas is a chaotic region where small variations of the initial conditions can lead the system to converge or diverge. On the contrary, when a saturation is added on the Poincaré maps, forcing A to stay positive, and for a value of λ lower than 0.4, the system is stable for any real positive values of V_0 and A_0.
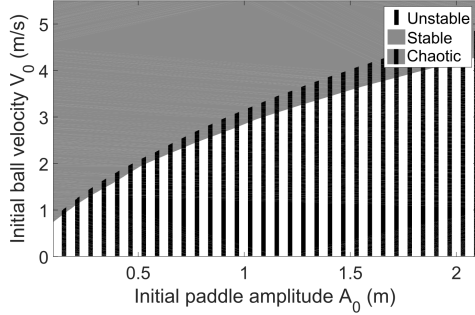

Figure 8: Attraction domain for $\alpha = 0.48$, $g = 9.81$, $\lambda = 0.09$, $\phi_0 = 0.5$. 400000 pairs are uniformly selected between predefined extreme values ($V_0 \in [-5,5]$ and $A_0 \in [0,2.2]$).

4.5 Comparison with a LQR Controller

A parrallel can be drawn between the proposed non-linear human-like controller and more traditional control methods. Considering the linearization of the high bounce map around an equilibrium point. The human-like controller takes the form of a linear state-feedback. An equivalent LQR controller formulation can be found. It is considered that the agent detects ϕ_0 at the first impact. For a specific $\bar{\phi} = \phi_0 \,(mod\,2\pi)$, there is only one equilibrium point given by the relation (7) that cancels the bounce error. It is thus possible to design a state feedback controller driving the state (A_k, V_k) towards the reference value $(\bar{A}, \bar{V})$. Here, a LQR controller controls the paddle amplitude whereas the paddle frequency is controlled to be equal to the ball frequency as in the previous sections. The LQR controller is designed based on the linearization of the map (11). The linear map can be written as:

$$\begin{pmatrix} X_{k+1} \\ U_k \end{pmatrix} = \begin{bmatrix} \tilde{A} & \tilde{B} \\ 0 & 1 \end{bmatrix} \begin{pmatrix} X_k \\ U_{k-1} \end{pmatrix} + \begin{bmatrix} \tilde{B} \\ 1 \end{bmatrix} \Delta U_k \qquad (15a)$$

$$Y_k = \begin{bmatrix} \tilde{C}_1 & \tilde{C}_2 \end{bmatrix} \begin{pmatrix} X_k \\ U_{k-1} \end{pmatrix} \qquad (15b)$$

with $X_k = V_k - \bar{V}$, $U_k = A_{k+1} - \bar{A}$, $Y_k = h_{a_k} - h_p$ and :

$$\tilde{A} = \left. \frac{\partial X_{k+1}}{\partial X_k} \right|_{\{\bar{A}, \bar{V}\}} = 2\alpha - 1 \qquad (16a)$$

$$\tilde{B} = \left. \frac{\partial X_{k+1}}{\partial U_{k-1}} \right|_{\{\bar{A}, \bar{V}\}} = (1+\alpha)\frac{\cos(\phi_0)\pi g}{\bar{V}} \qquad (16b)$$

$$\tilde{C}_1 = \left. \frac{\partial Y_k}{\partial X_k} \right|_{\{\bar{A}, \bar{V}\}} = \frac{\bar{V}}{g} \qquad (16c)$$

$$\tilde{C}_2 = \left. \frac{\partial Y_k}{\partial U_{k-1}} \right|_{\{\bar{A}, \bar{V}\}} = \sin(\phi_0) \qquad (16d)$$

Let Z_k be the state vector $\begin{pmatrix} X_k \\ U_{k-1} \end{pmatrix} \in \mathbb{R}^2$. A LQR controller $\Delta U_k = -[K_1 \; K_2] Z_k \;(\in \mathbb{R})$ can be derived for this linear map by solving a well-known Riccati equation (Kwakernaak and Sivan, 1972). This controller minimizes the cost function $\sum_{k=1}^{+\infty} Z_k^{\top} Q Z_k + R\Delta U_k^2$, with Q and R two positive matrices ($\in M_{2,2}(\mathbb{R})$).

The closed-loop LQR map is thus equal to:

$$A_{k+1} = K_2\bar{A} + (1 - K_2)A_k - K_1(V_k - \bar{V}) \qquad (17a)$$

$$V_{k+1} = \alpha V_k + (1+\alpha)A_{k+1}\pi g\cos(\phi_0)/V_k \qquad (17b)$$

It can be noticed that the human-like controller linearized around the equilibrium point has a form similar to the LQR one: $\Delta U_k = -\lambda Y_k = -\lambda(\tilde{C}_1 \; \tilde{C}_2)Z_k$.

The matrices Q and R were chosen so that the eigenvalues of (17) were equal to the one of the human-like bouncing map (11) (the eigenvalues of the later being equal to the ones of the linearized bouncing map (15) controlled by the linearized human-like controller). For $\lambda = 0.09, \phi_0 = 0.5, \alpha = 0.48$, the eigenvalues of (6) are $\{-0.0625, 0.6121\}$. For $Q = 0.013 \left(\tilde{C}_1 \quad \tilde{C}_2\right)^T \left(\tilde{C}_1 \quad \tilde{C}_2\right)$ and $R = 1$, the eigenvalues of (15) are $\{-0.0396, 0.6096\}$. It can be seen on the Bode plot of Figure 9 that the dynamics of the closed-loop systems controlled by the linear human-like controller and by the LQR controller are very similar. However, the LQR controller has the disadvantages of supposing that the relation between the equilibrium point and the initial conditions is known *a priori*, as it integrates $\bar{A}$ and $\bar{V}$ in (17a). The eigenvalues and the stability properties thus depend on h_p and g. In the other hand, the system (17) was converging for any real positive values of A_0 and V_0 tested. The attraction domain of the LQR controller is thus larger than the one of the human-like controller presented in Figure 8, for the environmental conditions tested.
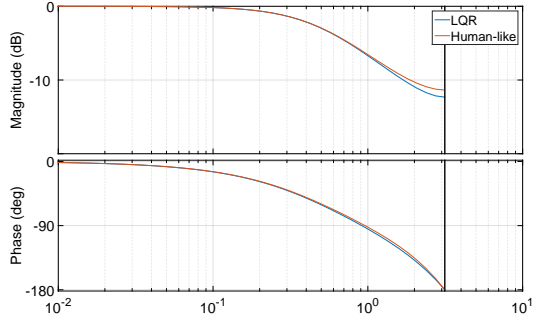
Figure 9: Bode plot of the closed-loop bouncing map for the LQR and the human-like controller.

5 POINCARÉ MAP WITH PHASE CONTROL

In the stability analysis of Section 4.3, the system was shown to be stable provided that λ is lower than an identified limit value. This stable bouncing was ensured even for positive paddle impact acceleration, i.e. outside the passive stability regime identified in (Dijkstra et al., 2004), (Schaal et al., 1996). However, as recalled in Section 2.2, participants were shown to generally hit the ball with an impact phase inside the passive stability regime, corresponding to a specific interval of negative paddle accelerations at impact. The question of whether this behavior is the result of a conscious strategy, with the impact phase actively controlled to converge towards this regime, or the result of an unconscious process resulting from the task passive dynamics themselves is investigated in the following paragraphs.

5.1 The Passive Hypothesis

In the present paragraph it is suggested that participants tuned into the passive stability regime, not intentionally, but actually because the paddle frequency control may not be always active. It can indeed be observed that if the frequency adaptation is switched off during a steady-state trial and that a very small perturbation is introduced on the paddle frequency, then either the ball impact phase converges toward the passive stability regime because of the passive dynamics of the task, or diverges. In the divergence case, the agent would switch the frequency adaptation back on to stabilize the bouncing. To evidence the passive convergence case, both numerical simulations of the task continuous dynamics and computations of the Poincaré map (6) predictions were performed. During the first 15 impacts of a trial, the paddle period was adapted to equal the ball period

on a cycle basis. Then the active frequency control is switched off and a small perturbation is added on the paddle frequency of frequency adaptation law $\omega_{k+1} = \pi g / V_k + randn/500$. The convergence towards the passive stability regime for both the simulation and the Poincaré map is shown in Figure 10 for two different values of ϕ_0. This Figure shows that during these two trials, after the active frequency control was switched off, the bouncing was indeed driven by the passive dynamics of the task towards the passive stability regime. The Poincaré map (6) accurately predicts this passive convergence observed with the continuous-time simulations. It can be noted that the convergence or divergence of the bouncing, after the active control is switched off, can be predicted by looking at the attraction domain of the open-loop Poincaré map presented in (Dijkstra et al., 2004).
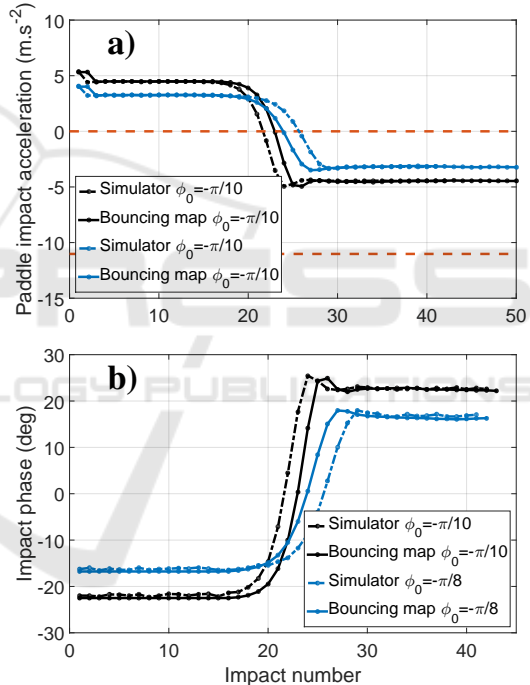

Figure 10: Examples of trials converging towards a new limit cycle inside the passive stability regime when the frequency control is switched off a) Paddle acceleration at impact. The red dashed lines represent the upper and lower values of the passive stability regimes for the mathematical expression given in (Dijkstra et al., 2004) b) Impact phase ($\lambda = 0$, $A_0 = 0.15$).

5.2 The Active Control Hypothesis

In this Section, in addition to the active control of the ball amplitude, the ball-paddle phase at impact is considered to be controlled through an adaptation of the paddle frequency control of (5a). The paddle period is adapted on a cycle basis so that $T_r(k+1) =$

$T_b(k+1) + \sigma(\phi_k - \phi^*)$, with ϕ^* the objective impact phase and σ an adaptation coefficient. The Poincaré map is thus given by (18):

$$\omega_{k+1} = \frac{2\pi}{\sigma(\phi_k - \phi^*) + 2V_k/g} \tag{18a}$$

$$A_{k+1} = A_k + \lambda(h_p - A_k \sin(\phi_k) - \frac{V_k^2}{2g}) \tag{18b}$$

$$V_{k+1} = -\alpha V_k + (1+\alpha)A_{k+1}\omega_{k+1}\cos(\phi_{k+1})$$
$$+ \frac{\alpha g}{\omega_{k+1}}(\phi_{k+1} - \phi_{k+1}) \tag{18c}$$

$$A_{k+1}\sin(\phi_{k+1}) = A_k \sin(\phi_k) + \frac{V_k}{\omega_{k+1}}(\phi_{k+1} - \phi_k)$$
$$- \frac{g}{2\omega_{k+1}^2}(\phi_{k+1} - \phi_k)^2 \tag{18d}$$

The comparison of the ball bouncing performances predicted by the bouncing map (18) to simulations led to an accurate matching and highlights the relevance of the task stability analysis focused on the discrete-time dynamics. An example of such comparison is given in Figure 11.

The Jacobian matrix takes the same form as in (9), with the same state. The eigenvalues of the Jacobian matrix evaluated at the equilibrium point have complex expressions that will not be presented in the present paper. Figure 12 represents the influence of λ, σ and $\bar{\phi} = \phi^*$ on the Jacobian absolute eigenvalues. It can be seen that the third eigenvalue, that was non-hyperbolic in Section 3.2 ($|ev_3| = 1$), is now hyperbolic and always stable ($|ev_3| < 1$) (Figures c) and f)). The first eigenvalue is stable for $\sigma < 0.3$ and $\lambda < 0.4$ (Figures b) and e)). For $\sigma < 0.3$, the second eigenvalue is stable for any value of λ. To summarize, the active impact phase control does not provide additional stability to the system (the limit value of λ is the same than the one without active phase control, according to Figure 12d)), and requires an *a priori* knowledge of ϕ^*. However, it is interesting to note that with active phase control, the Poincaré map is not singular anymore and the equilibrium point is unique. It is possible to conclude that the equilibrium point defined by relations (7) and $\bar{\phi} = \phi^*$ is asymptotically stable without the need for Poincaré map approximation. The influence of α on the real and imaginary parts of the three eigenvalues is shown in Figure 13.

6 CONCLUSIONS

The ball-bouncing task has in several past studies constituted a benchmark to analyze the generation of rhythmic movement in humans. Previous experimental studies proposed hypotheses about amplitude, period and phase adaptation laws, that were confronted
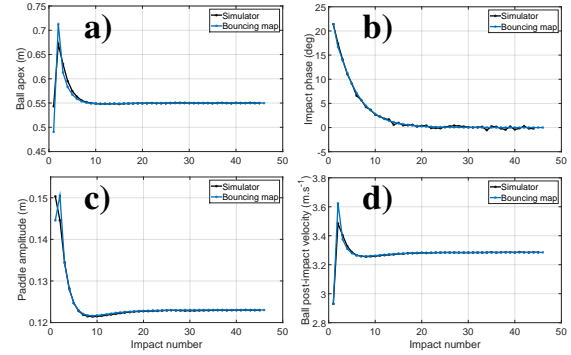

Figure 11: Example of comparison of the bouncing performances simulated and predicted by the Poincaré map with a) the apex series, b) the phase series, c) the paddle amplitude series, d) the ball velocity after impact series. Here $\lambda = 0.09$, $\sigma = 0.05$, $\phi^* = 0.5$.
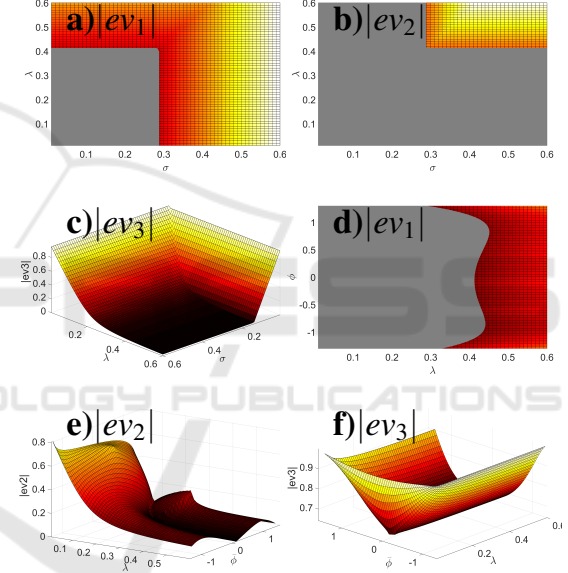

Figure 12: For different values of σ ($\alpha = 0.48$, $\lambda = 0.09$), a) represents $|ev_1|$, b) $|ev_2|$, c) $|ev_3|$. For different values of λ ($\alpha = 0.48$, $\sigma = 0.05$), d) represents $|ev_1|$, e) $|ev_2|$, f) $|ev_3|$. The gray area on Figures a), b), d) corresponds to $|ev| < 1$ (stable area). Figures c), e) and f) are represented in 3D plots because the corresponding eigenvalue is always lower than unity.

to an asymptotic stability analysis in the present study. Conclusions about their verisimilitude were derived and their stability consequences were identified.

The human adaptation strategies of the paddle oscillation amplitude and period were shown to efficiently stabilize the bouncing map. The equilibrium points stability was assessed for values of the discrete-time integrator coefficient λ lower than a limit value 0.4. The nonlinear human-like controller was shown to be equivalent to a LQR controller around an equilibrium point, while requiring no *a priori* knowledge
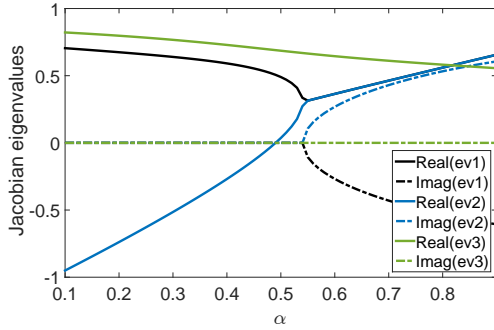
Figure 13: Real and imaginary parts of the Jacobian eigen-values, as a function of α, for the bouncing map with active phase control ($\lambda = 0.09$, $\sigma = 0.05$, $\phi^* = 0.5$).

about the equilibrium point.

Notwithstanding the stability of the task with active amplitude and frequency control assessed in the present paper, participants are shown to hit the ball in the passive stability regime (Sternad et al., 2001). The present papers analyzed two alternatives justifications: the impact phase is either actively controlled by participants or unconsciously driven by the passive dynamics of the task. The study showed that the active impact phase control does not increase stability that would otherwise justify a voluntary control. It is also shown that if at one moment of the trial the active frequency control is switched off, then the paddle acceleration is driven by the passive dynamics of the task and goes back to the passive stability regime. This second hypothesis thus seems more likely to explain the observed human behavior.

Finally, the efficient prediction of the human control strategies stability was achieved without simulating the whole continuous and discrete dynamics of the system. For robotic applications, with the objective of identifying the control paradigm that gives humans such a dexterity to achieve tasks in interaction with the environment, the present study proposes a method to discard unnecessary control hypotheses while facilitating the controller adaptation coefficients setting. The method can be extended to other tasks involving repeated robot-environment interactions and reduces the computation time of the robustness tests by avoiding simulation of the task continuous dynamics.

ACKNOWLEDGEMENTS

REFERENCES

Avrin, G., Makarov, M., Rodriguez-Ayerbe, P., and Siegler, I. A. (2016). Particle swarm optimization of Matsuoka's oscillator parameters in human-like control of rhythmic movements. In *Proc. IEEE American Control Conf.*

Buehler, M., Koditschek, D. E., and Kindlmann, P. (1990). A simple juggling robot: Theory and experimentation. In *Exp. Rob. I*, pages 35–73. Springer.

Choudhary, S. K. (2016). Lqr based optimal control of chaotic dynamical systems. *Int. J. of Modelling and Simulation*, 35(3-4):104–112.

de Rugy, A., Wei, K., Müller, H., and Sternad, D. (2003). Actively tracking passive stability in a ball bouncing task. *Brain Research*, 982(1):64 – 78.

Dijkstra, T., Katsumata, H., de Rugy, A., and Sternad, D. (2004). The dialogue between data and model: passive stability and relaxation behav. in a ball-bouncing task. *Nonlinear Studies*, pages 11:319–344.

Holmes, P. J. (1982). The dynamics of repeated impacts with a sinusoidally vibrating table. *J. of Sound and Vibration*, 84(2):173–189.

Kulchenko, P. and Todorov, E. (2011). First-exit model predictive control of fast discontinuous dynamics: Application to ball bouncing. In *Robotics and Auto. (ICRA), 2011 IEEE Int. Conf. on*, pages 2144–2151. IEEE.

Kwakernaak, H. and Sivan, R. (1972). *Linear optimal control Systems*, volume 1. Wiley-interscience New York.

Morice, A., Siegler, I. A., Bardy, B., and Warren, W. (2007). Action-perception patterns in virtual ball bouncing: combating syst. latency and tracking functional validity. *Experimental Brain Research*, pages 181:249–265.

Ronsse, R. and Sepulchre, R. (2006). Feedback control of impact dynamics: the bouncing ball revisited. In *Proc. of the 45th IEEE Conf. on Decision and Control*, pages 4807–4812. IEEE.

Schaal, S., Sternad, D., and Atkeson, C. G. (1996). One-handed juggling: A dynamical approach to a rhythmic movement task. *J. of Mot. Behav.*, 28(2):165–183.

Siegler, I. A., Bardy, B. G., and Warren, W. H. (2010). Passive vs. active control of rhythmic ball bouncing: the role of visual information. *J. of Exp. Psychol. Hum. Percept. and Perform.*, 36(3):729–50.

Siegler, I. A., Bazile, C., and Warren, W. (2013). Mixed control for perception and action: timing and error correction in rhythmic ball-bouncing. *Exp. Brain Res.*, 226(4):603–615.

Sternad, D., Duarte, M., Katsumata, H., and Schaal, S. (2001). Bouncing a ball: tuning into dynamic stability. *J. of Exp. Psychol. Hum. Percept. and Perform.*, 27(5):1163.

Stuart, A. and Humphries, A. R. (1998). *Dynamical systems and numerical analysis*, volume 2. Cambridge University Press.

Tufillaro, N., Mello, T., Choi, Y., and Albano, A. (1986). Period doubling boundaries of a bouncing ball. *J. de Physique*, 47(9):1477–1482.

Vincent, T. L. (1995). Controlling a ball to bounce at a fixed height. In *American Control Conf., Proc. of the 1995*, volume 1, pages 842–846. IEEE.

Vincent, T. L. and Mees, A. I. (2000). Controlling a bouncing ball. *Int. J. of Bifurcation and Chaos*, 10(03):579–592.

Williamson, M. (1999). Designing rhythmic motions using neural oscillators. In *Proc. IEEE/RSJ Int. Conf. on Intelligent Robots and Syst.s (IROS)*, volume 1, pages 494–500 vol.1.

Yu, J., Tan, M., Chen, J., and Zhang, J. (2014). A survey on CPG-inspired control models and syst. implementation. *IEEE Trans. Neural Netw. Learn. Syst.*, 25(3):441–456.